Journal of Magnetics 5(3), 85-89 (2000)

# Analysis of Hysteretic Giant Magnetoimpedance Using Stoner-Wohlfarth Model

**K. J. Jang[1,3], C. G. Kim[1], D. Y. Kim[2] and C. O. Kim[3]**

[1]*Department of Physics and Advanced Material Science, Sun Moon University, Chungnam 336-840, Korea*
[2]*Telecomm. systems SBU, Hyundai Electronics Co., Ltd, Ichon, Kyoungki 476-860, Korea*
[3]*Research Center for Advanced Magnetic Materials, Chungnam National University, Taejon 305-764, Korea*

(Received 1 August 2000)

**The hysteretic characteristics of giant magnetoimpedance (GMI) profiles have been measured in Co-based amorphous ribbon with various anisotropy angles $\theta_k$, and they have been analyzed by using the Stoner-Wohlfarth model. Two-peaks behavior with a dip near zero field is revealed in the measured GMI profile at 10 MHz irrespective of $\theta_k$. The negligible hysteresis of the field for the dip is close to the calculation assuming the magnetization jump from a metastable to stable state. However, the hysteretic asymmetry for the angle range of $20^\circ \leq \theta_k < 60^\circ$ is well described by the divergence in the calculation without the magnetization jump. The asymmetry for $\theta_k \geq 60^\circ$ may be due to the divergence, but the shapes of measured profiles are quite different from the calculations with single peak near zero field, indicating that Stoner-Wohlfarth model can be well used to describe GMI characteristics for the anisotropy angle range of $20^\circ \leq \theta_k < 60^\circ$ at the frequency of 10 MHz in Co-based amorphous ribbons.**

## 1. Introduction

Since the discovery of a giant magnetoimpedance (GMI) effect, much work has been performed on the GMI in soft magnetic Co- and Fe-based amorphous ribbon and wires in view of academic interest and practical applications [1, 2], where the GMI is the effect of the magnetic field on the transverse permeability in the direction of ac measuring current. The sensitivity and linearity for the magnetic field are the most important parameters in the practical application of GMI for magnetic sensors. For the theoretical works on the GMI for varying magnetic anisotropies, there are two kinds of models to calculate transverse permeability from rotational magnetization [3-6].

One of theoretical models is dealt with the induced volatge as a function of impedance tensor during the magnetization [3, 4], because the GMI is phenomenologically understood as a sensitive change of ac voltage across the two terminals in the materials subjected to an ac current and quasistatic magnetic field. Calculating the impedance tensor fot ratational magnetization with the help of Maxwell equation, the symmetric two-peaks of induced voltage are revealed during a half cycle of magnetization in the magnetic material with an uniaxial anisotropy. Whereas the voltage exhibits the asymmetric behavior in the material with two kinds of anisotropies.

Another model is based on the quasistatic magnetization due to the rotational magnetization for the transverse permeability, known as Stoner-Wohlfarth model [5]. When the magnetization under the field is assumed to jump from a metastable to stable state, that is, by taking the minimum energy condition, the calculated profiles during the magnetization are quite similar to the induced volatge using impedance tensor according to the anisotropy parameters. Furthermore, asymmetric GMI profiles are qualitatively well ascribed by the modified Stoner-Wohlfarth model which introduces an uniaxial and unidirectional anisotropies [6]. However, there is still discussion for the validity of Stoner-Wohlfarth model according to the calculation method [7, 8].

In this work, GMI profiles have been measured in the Co-based amorphous ribbons with the varying anisotropy angles and compared to the calculation using the Stoner-Wohlfarth model in order to evaluate the validity of the model.

## 2. Modeling

Let's consider the Stoner-Wohlfarth model [9] for the rotation of single domain under the uniaxial anisotropy to calculate transverse permeability, as shown in Fig. 1. Here, an uniaxial anisotropy is inferred to the corresponding one for the randomly distributed local anisotropy with a preferred direction. The external field $H$ and ac current $I$ act along the ribbon axis, and $H_t$ is transverse field produced by the ac current. The uniaxial easy axis makes an angle $\theta_k$ from the transverse direction. The energy for magnetization $M_s$ tilted away from easy axis by angle $\theta$ is written as

$$E = K\sin^2(\theta - \theta_k) - M_s H_t \cos\theta - H M_s \sin\theta \quad (1)$$

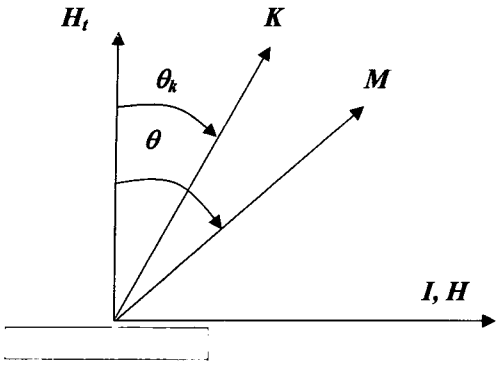


Fig. 1. Coordinate system for rotational magnetization under uniaxial anisotropy.

where $K$ is an uniaxial anisotropy constant. After some partial derivative procedures with change of variables and taking small $H_t$ field approximation, the rotational transverse susceptibility $x_t$ is obtained as following [5];

$$\chi_t(H)=\frac{M_s\sin^2\theta}{H_k\cos 2(\theta-\theta_k)+H\sin\theta} \tag{2}$$

where we define anisotropy field $H_k=2K/M_s$. We can figure the GMI profile from the $x_t(H)$ because the GMI at high frequency can be written as

$$Z(H)\propto\sqrt{\mu_t(H)} \tag{3}$$

where $\mu_t=1+4\pi\chi_t$ is transverse magnetic permeability.

Figure 2 shows the energy curves for the parameters, $\theta_k=-30^\circ$ and $H_k=3$ Oe according to magnetization angle under the various fields. When the equilibrium angle $\theta(H)$ is determined in the minimum energy condition during the decreasing field, that is, assuming the magnetization jump from metastable to stable state, then the equilibruin angle changes as following states a → b → c' → d. In this case, there is no hysteresis in the magnetization in longitudinal direction for increasing and decreasing fields, as in Fig. 3. Here, the magnetization is obtained by taking $\cos\theta(H)$. When the angle of magnetization under the field remains a metastable state without jumping, following the states a → b → c → d, then a hysteresis is revealed in the magnetization, as shown in Fig. 3.

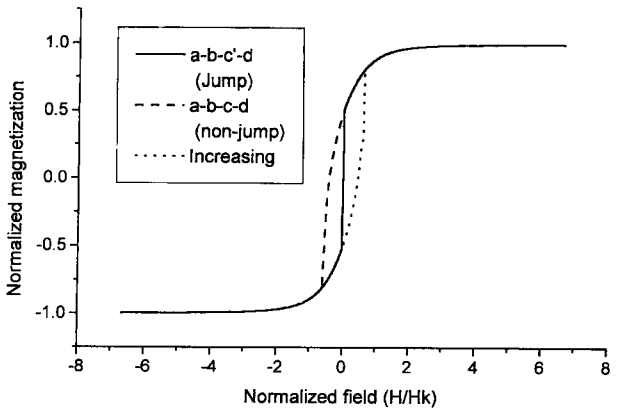


Fig. 3. Calculated magnetization curves for the different magnetization paths.

Figures 4(a) and (b) show the numerically obtained GMI profiles for the fitting parameter, $\theta_k=10^\circ$. The equilibrium angle $\theta(H)$ in eq. (1) is determined for the minimum energy condition, then, symmetric two-peaks of GMI are revealed at $H\cong\pm H_k$ for increasing and decreasing fields, respectively, without the hysteresis as in Fig. 4(a). The shape of profile remains up to the angle of 50° even though there is a little change in the field interval of two peaks. These profile characteristics are the same as the theoretically obtained one using the impedance tensors for inductive voltage [3].

However, the angle of magnetization is assumed to remain in a metastable state without jumping, then the profile shows the asymmetry with the divergence at the values of the field $H\approx+0.58H_k$, $-0.58H_k$, as indicated by arrows in Fig. 4(b), for increasing and decreasing fields, respectively. At these fields, the magnetization angle is at inflection point in $E(\theta)$-curve, i.e., $\partial^2E/\partial\theta^2=0$. In this case, there is also a hysteresis in the field $H_{hyst}$ at which the dip of GMI profile occurs.

The calculated GMI profiles are shown in Figs. 5(a) and

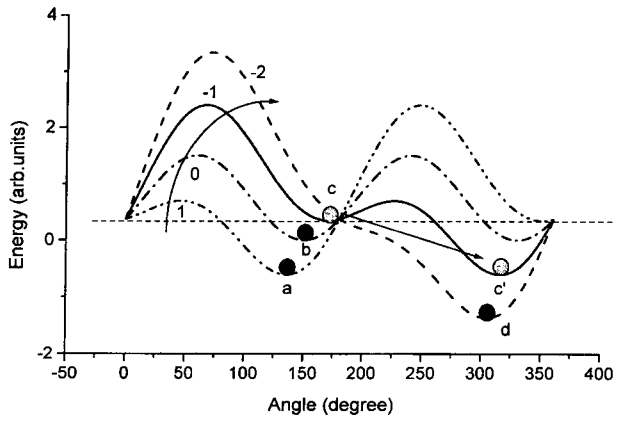


Fig. 2. Energy variation according to the direction of magnetization under several magnetic fields.

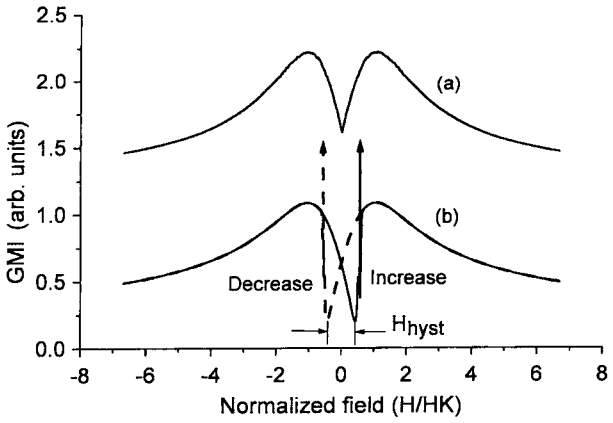


Fig. 4. Calculated GMI profile ($\sqrt{\mu_t}$) for the magnetization (a) with jump and (b) without jump at $\theta_k=10^\circ$.

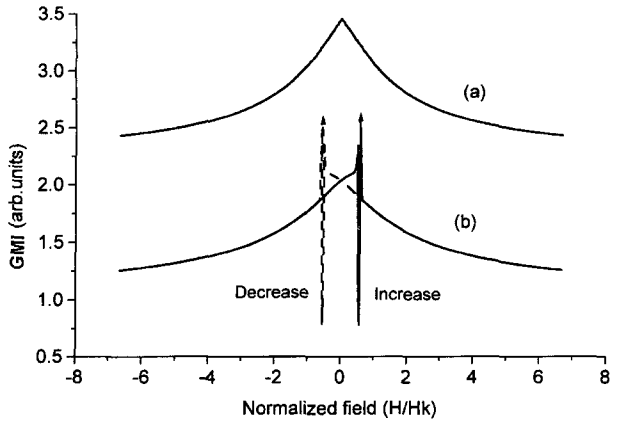


Fig. 5. Calculated GMI profile ($\sqrt{\mu_t}$) for the magnetization (a) with jump and (b) without jump at $\theta_k = 60°$.

(b) for the fitting parameter, $\theta_k$=60°. In the minimum energy condition, one peak of GMI for $\theta_k \geq 60°$ is shown without the hysteresis as in Fig. 5(a). However, the angle of magnetization, is assumed to remain in a metastable state without jumping, then the profile also shows the asymmetry with the divergence, as indicated by arrows in Fig. 5(b), and the center of peaks shifts to positive and negative fields for increasing and decreasing fields, respectively. There may be an effect of distributions in anisotropy magnitude and orientation [10]. Thus it is expected that there is an increase of GMI around the divergence points.

## 3. Experiment

A set of rectangular samples of $Co_{66}Fe_4B_{15}Si_{15}$ (15 $\mu$m thick, 2 mm wide, and 50 mm long) were annealed at 180 °C under the applied magnetic field $H_a$. Two components of magnetic field were controlled by two-dimensional Helmholtz coils. The magnitude of resultant field (vector sum) was 60 Oe and the angles $\theta_k$ from transverse direction were varied from 0° to 90°. The absolute value of complex impedance, $Z$, was measured by using an impedance analyzer (HP4192A) with four terminal contacts. The cyclic magnetic field $H$ was applied to the ribbon axis by Helmholtz coil using step-like changing current. The amplitude of ac prove current was kept at a constant value of 5 mA during the cyclic sweep of $H$.

## 4. Results and Discussion

Figures 6(a) and (b) show the measured GMI profiles $Z(H)$ at frequency $f = 0.1$ and 10 MHz for annealing-field angles $\theta_k$=10° and 60°, respectively. At $f = 0.1$ MHz, $Z(H)$ for the sample of $\theta_k$=10° shows typical two peaks located at positive and negative field, $H_{+p}$ and $H_{-p}$, while the profile in sample of $\theta_k$=60° shows a small dip at $H = 0$. At high frequency of 10 MHz, the dip of $Z(H)$ is profound irrespective of $\theta_k$.

The GMI is dominated by the wall motion in the low-frequency of 0.1 MHz. As the frequency increase above a few MHz in Co-based amorphous materials, the wall motion is damped, and the rotational magnetization is responsible for the GMI effect [3, 11]. Because Stoner-Wohlfarth model is based on the quasistatic rotational magnetization, the GMI profile at 10 MHz could be comparable to the calculation. There are overall agreements in two peaks behavior of the measured and calculated profiles for $\theta_k$=10° in Figs. 6(a) and 4, respectively. However, two peaks of GMI in Fig. 6(b)

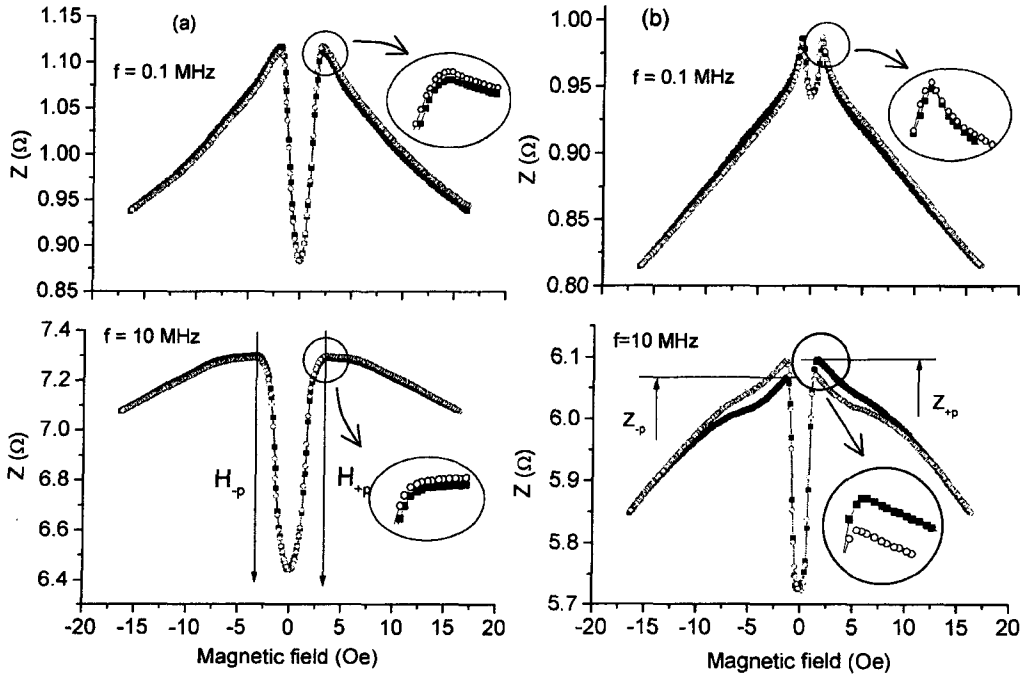


Fig. 6. Measured GMI profile in 0.1, 10 MHz for (a) $\theta_k = 10°$, and (b) $\theta_k = 60°$ ( ■ : increasing, ○ : decreasing fields).

is quite different from the calculations for $\theta_k$=60° in Fig. 4, regardless of magnetization jump and non-jump cases.

As can be seen in the inset figures, there is always a small hysteresis in the profiles for increasing and decreasing fields, causing the asymmetry. Here, we define the asymmetry ratio as the fractional difference between the impedance at two peaks, $\Delta Z_p/Z_{+p}$ as following;

$$\Delta Z_p/Z_{+p}+\lfloor Z_{+p}-Z_{-p}\rfloor/Z_{+p}\times 100(\%) \quad (4)$$

where $Z_{-p}$ and $Z_{+p}$ are the impedance values at the field of peaks $H_{-p}$ and $H_{+p}$, as depicted in Fig. 6(b), in the negative and positive field regions, respectively.

The variation of asymmetry ratio $\Delta Z_p/Z_{+p}$ with $\theta_k$ at 0.1 and 10 MHz is shown in Fig. 7(a) and (b), respectively. For the increasing part of cyclic applied field at 0.1 MHz, the sign of $\Delta Z_p/Z_{+p}$ is negative irrespective of $\theta_k$, which means that the peak at $H_{-p}$ is higher than that at $H_{+p}$. However, the sign of $\Delta Z_p/Z_{+p}$ is positive for the decreasing field. These asymmetric behaviors may be caused by the hysteresis of the domain wall motion.

For 10 MHz measuring frequency, the sign of $\Delta Z_p/Z_{+p}$ is negative for $\theta_k \leq 10°$ during increasing field (region I), however, the sign becomes positive for $\theta_k \geq 20°$ (region II, III). The variation of $\Delta Z_p/Z_{+p}$ for the decreasing part has an opposite tendency to these of the increasing part. The negligible hysteresis of field of dip, $H_{hyst}$ is more close to the calculation with the magnetization jump, rather than the calculation without the magnetization jump. However, the signs of $\Delta Z_p/Z_{+p}$ in regions II are well ascribed for by the presence of divergence in the calculation without the magnetization jump. In region III, the asymmetry may be due to the divergence, but the shapes of measured profiles are quite different from the calculations, as described before. This difference may be due to the distributions of the anisotropy magnitude and anisotropy angles in the actual materials.

The opposite sign in region I may be due to the small contribution of magnetization rotation on GMI because the most of sample volume for $\theta_k \leq 10°$ has the magnetization along the transverse direction to cause the wall motion. In view of asymmetry and shape, it is concluded that GMI characteristics for region II ($20° \leq \theta_k < 60°$) are well described by the calculation using Stoner-Wohlfarth model.

## 5. Conclusion

The hysteretic characteristics of giant magnetoimpedance (GMI) profiles have been measured in Co-based amorphous ribbon with the various anisotropy angles $\theta_k$ and compared to the calculation using the Stoner-Wohlfarth model. When the magnetization under the field is assumed to jump from a metastable to stable state, then the calculation reveals the symmetric two-peaks of GMI profiles for $\theta_k < 60°$, and one peak for $\theta_k \geq 60°$. However, the angle of magnetization is assumed to remain in a metastable state without jumping,

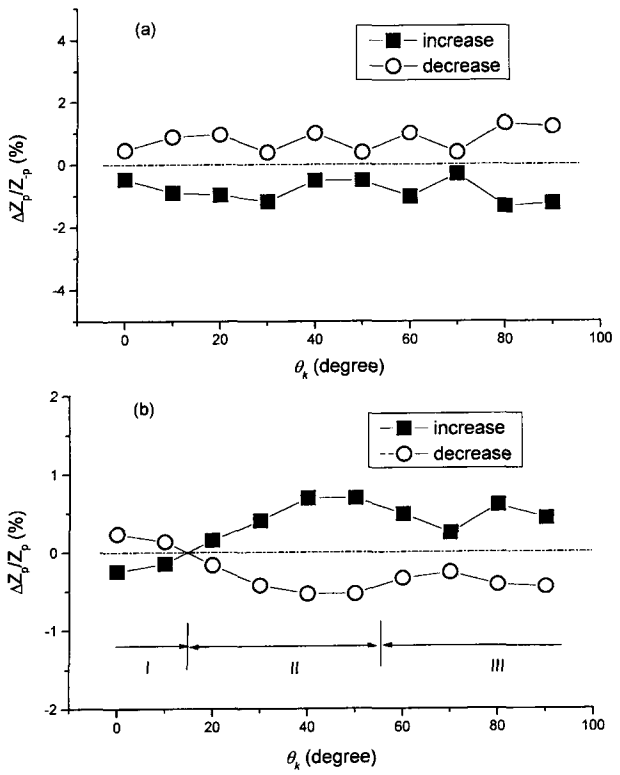


Fig. 7. Asymmetry ratio with the anisotropy angle of $\theta_k$ for (a) 0.1, (b) 10 MHz measuring frequencies

then the profile shows the divergence in positive and negative field regions for increasing and decreasing fields, respectively, where the divergence indicates the asymmetry and hysteresis in the GMI profile.

The negligible hysteresis of the field of dip in the measured GMI profiles is more close to the calculation with the magnetization jump. However, the asymmetry characteristics for the anisotropy angle range of $20° \leq \theta_k < 60°$ are well described by the divergence in the calculation without the magnetization jump. The asymmetry for $\theta_k \geq 60°$ may be due to the divergence but the shapes of measured profiles are quite different from the calculations. From the view of asymmetry and shape of GMI profiles, it is concluded that Stoner-Wohlfarth model can be well used to describe GMI characteristics for the anisotropy angle range of $20° \leq \theta_k < 60°$ at the frequency of 10 MHz, and the developing model to explain the GMI for $\theta_k \leq 10°$ becomes an interesting work to be further studied.

## Acknowledgements

This work was supported by the Korean Science and Engineering Foundation through the Research Center for Advanced Magnetic Materials at Chungnam National University.

## References

[1] K. Mohri, K. Kawashima, T. Kohzawa, Y. Yoshida, and

L. V. Panina, IEEE Trans. Magn., **28**, 3150 (1992).
[2] C. G. Kim, K. J. Jang, H. C. Kim, and S. S. Yoon, J. Appl. Phys., **85**, 5447 (1999).
[3] L. V. Panina, K. Mohri, T. Uchiyama, M. Noda, and K. Bushida, IEEE Trans. Magn., **34**, 1249 (1995).
[4] D. P. Makhnovskiy, L. V. Panina, and D. J. Mapps, J. Appl. Phys., **87**, 4804 (2000).
[5] S. S. Yoon, S. C. Yu, K. H. Ryu, and C. G. Kim, J. Appl. Phys., **85**, 5432 (1999).
[6] C. G. Kim, K. J. Jang, D. Y. Kim, and S. S. Yoon, Appl. Phys. Lett., **75**, 2114 (1999); C. G. Kim, K. J. Jang, D. Y. Kim, and S. S. Yoon, Appl. Phys. Lett., **76**, 1345 (2000)
[7] D. X. Chen, L. Pascual, and A. Hernando, Appl. Phys Lett., **77**, in press, #LN00-0962 (2000).
[8] C. G. Kim, K. J. Jang, D. Y. Kim, and S. S. Yoon, Appl Phys. Lett., **77**, in press, #LN00-1484 (2000).
[9] A. Hubert and R. Schafer, Magnetic domains, (Springer-Verlag, Heidelberg, 1998), pp. 201-214.
[10] P. T. Squire, J. Magn. Magn. Mater., **87**, 299 (1990).
[11] S. S. Yoon, C. G. Kim, H. C. Kim, K. J. Jang, and K. S Ryu, J. Magn. Mag. Mater., **203**, 301 (1999).